Separation Science and Technology
Publication details, including instructions for authors and subscription information:
http://www.informaworld.com/smpp/title~content=t713708471

Modeling of the Mass Transfer Rates of Metal Ions across Supported Liquid Membranes. I. Theory

A. A. Elhassadi; D. D. Do[a]
[a] DEPARTMENT OF CHEMICAL ENGINEERING, UNIVERSITY OF QUEENSLAND, ST. LUCIA, QUEENSLAND, AUSTRALIA

Online publication date: 29 January 1999

To cite this Article Elhassadi, A. A. and Do, D. D.(1999) 'Modeling of the Mass Transfer Rates of Metal Ions across Supported Liquid Membranes. I. Theory', Separation Science and Technology, 34: 2, 305 — 329
To link to this Article: DOI: 10.1081/SS-100100652
URL: http://dx.doi.org/10.1081/SS-100100652

SEPARATION SCIENCE AND TECHNOLOGY, **34**(2), pp. 305–329, 1999

Modeling of the Mass Transfer Rates of Metal Ions across Supported Liquid Membranes. I. Theory

A. A. ELHASSADI*
DEPARTMENT OF CHEMISTRY
UNIVERSITY OF GARYOUNIS
BENGHAZI, LIBYA

D. D. DO
DEPARTMENT OF CHEMICAL ENGINEERING
UNIVERSITY OF QUEENSLAND
ST. LUCIA, QUEENSLAND 4067, AUSTRALIA

ABSTRACT

This paper deals with the modeling of the transport and separation of metal ions across supported liquid membranes. The mass transfer resistance at the liquid–membrane interfaces and the interfacial chemical reactions at both the extracting side and the stripping side are taken into account in the model equations. Simple analysis of the time scale of the system shows the influence of various important parameters and their interactions on the overall transport rate. Parametric studies are also dealt with in this paper.

INTRODUCTION

Supported liquid membranes (SLMS) containing active carriers provide a simple, stable means for studying the transport, concentration, and selective separation of metals from dilute aqueous solutions (1). This simple geometry also provides a good means for understanding the fundamental aspects of the kinetics of such systems. The most frequent applications of liquid membrane systems have been in the concentration and selective separations of heavy

* To whom correspondence should be addressed. Present address: c/o Ashref M. Dardi, 42-31 Centennial Street, Regina, SK S4S 6P8, Canada.

metal ions. Heavy metals such as uranium and thorium are very important energy sources (2–4).

Supported liquid membranes are usually prepared by filling the pores of these membranes with the organic liquid composed of the carrier and the diluent. In order to insure that all the pores of the membrane are effectively filled, the membrane is immersed in the organic solution under vacuum. This simple geometry, which is economical for research purposes, uses a very small amount of organic solution to transport large amounts of metal ions. The disadvantage of flat supported liquid membranes is their small contact surface area per unit volume. As such, the SLM is analogous to the separating funnel used in solvent extraction, but the process is a simultaneous extraction–stripping one.

In this paper we propose a mechanism for the transport of metal ions through a SLM. The following steps are necessary:

1. Distribution of the metal from the aqueous phase to the liquid membrane phase (i.e., the diluent, the carrier, or their mixture). The distribution coefficient of the metal ions from the aqueous source solution into the membrane organic phase (K_{d1}) should be high enough to favor metal distribution into the membrane phase.
2. Either (a) passive diffusion of the metal through the diluent or (b) the metal combines with the carrier and the resulting complex diffuses across the membrane.
3. At the other side of the membrane, the distribution coefficient of the metal ions from the membrane liquid phase into the sink aqueous phase (i.e., K_{d2}) should be low enough to favor stripping into the sink solution.
4. Return of the carrier across the membrane.

This mechanism and the concentration profiles are schematically illustrated in Figs. 1 and 2. The proposed mechanism is different than the mechanism proposed by Komasawa et al. (5) who assumes the distribution of the carrier from the organic into the aqueous phase complexes with the metal ions. This description cannot be accepted because it violates the integrity of the impregnated membrane.

Numerous workers have mathematically modeled these liquid membrane systems. The previous developments have approached the problem in two ways. The first approach restricted the analysis to the limiting case of fast chemical reactions at the interfaces. This caused local equilibrium to take place, and hence very simple chemical thermodynamic models were constructed. Lee et al. (6) utilized this model and assumed the flux of the metal–carrier complex is proportional to half the average concentration of the carrier in the membrane. For the competitive transport of two metals, the relative fluxes were proportional to their relative concentrations in the aqueous

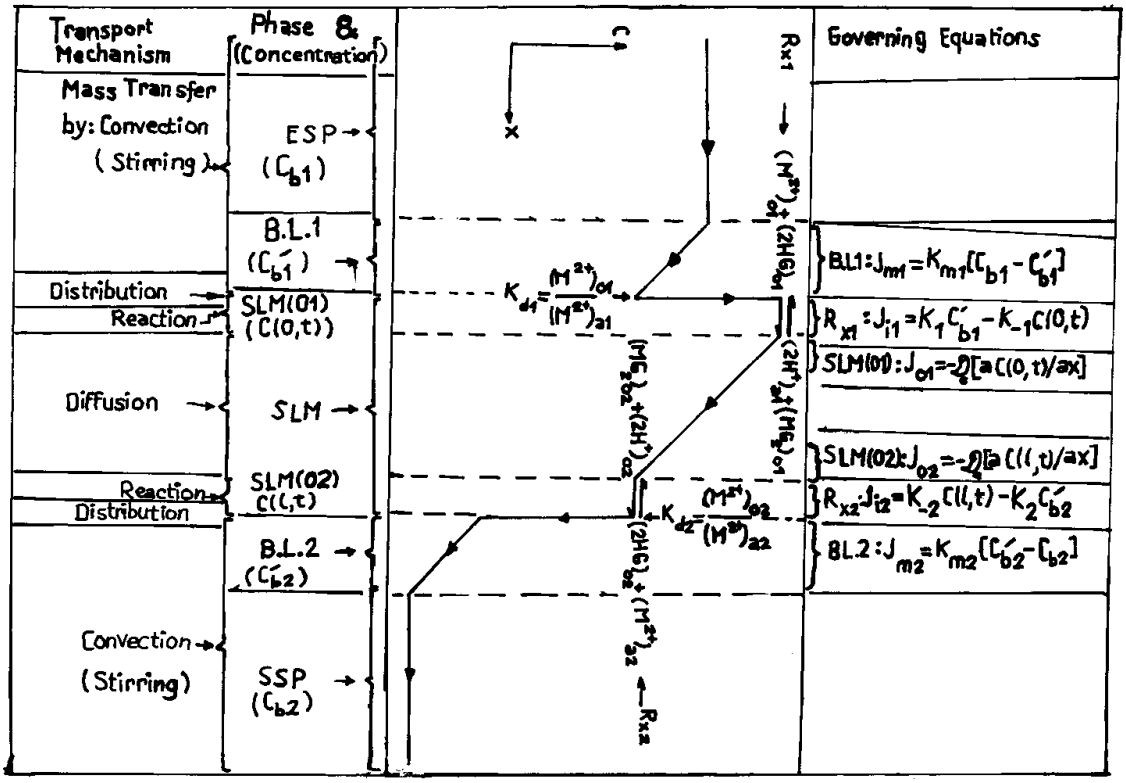

FIG. 1 Schematic description of transport phenomena and mechanisms, concentration profiles, phase regions, and governing equations of coupled transport of a divalent metal cation M^{2+} across a SLM.

phase. The model was not applicable at high values of carrier concentration where the flux no longer varies linearly with carrier concentration but rather it approaches a limiting value.

Second, Danesi et al. (7) were able to explain this limiting flux behavior by incorporating diffusional resistance within the membrane, interfacial reaction resistance, and aqueous diffusional resistance within the aqueous boundary layer. Their analysis was restricted to the steady-state behavior of the system. Their model equation failed to explain the behavior beyond the maximum limiting flux and did not couple the SLM material balance with the material balances of the two reservoirs. Kopp et al. (8) approached a similar problem of diffusion and reaction in an emulsion globule by examining the analogous planar problem with constant bulk solute concentration.

Clearly a detailed mathematical model is necessary to describe the transport processes controlling the extraction, the diffusion, and the stripping rates more accurately. The new model is a significant improvement over existing models

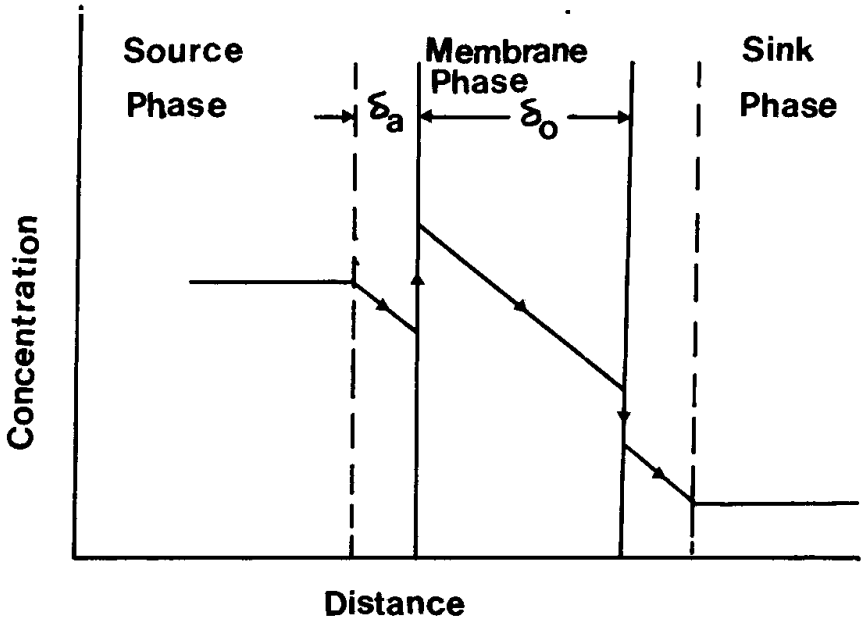

FIG. 2 Schematic representation of the linear concentration profiles within the aqueous extraction boundary layer, the organic membrane matrix, and the aqueous stripping boundary layer.

because it is more comprehensive and can be applied easily to continuous flow experiments and can be used for design purposes.

A detailed study of the extraction of naphthenic acid from kerosene was carried out using both porous and nonporous membranes. An attempt was made to determine the intrinsic membranes mass transfer characteristics as in Table 1 (9).

Juang investigated the phenomenon of uphill VO^{2+} transport experimentally and compared it with the results of a model considering all possible resistances. The degree of uphill transport remains relatively larger for either higher (pumping ion ratio) or lower (transported ion ratio) values. Both correspond to situations where the role of membrane diffusion becomes more

TABLE 1
Intrinsic Membranes Mass Transfer Characteristics

Membrane	Type	ϵ	δ	D_0 ($m^2 \cdot s^{-1}$)	K_m ($m \cdot s^{-1}$)	τ
Tetratec	Porous	0.85	38×10^{-6}	6.23×10^{-10}	4.17×10^{-6}	3.35
Celgard	Porous	—	—	—	—	2
PDMS	Nonporous	—	40×10^{-6}	6.78×10^{-11}	1.7×10^{-6}	—

MARCEL DEKKER, INC.
270 Madison Avenue, New York, New York 10016

important compared to aqueous layer diffusion and interfacial chemical reaction (10).

Darbi (11) studied the transport of iron and manganese through a SLM using a solubility mechanism model which predicts the permeability behavior with respect to carrier concentration. The optimal ratios of distributing the metal ions into the diluent (β) over that into the carrier (α) is about four times for both metals.

Hassan (12) analyzed the transport of manganese across a SLM using a viscosity effect model which predicts the experimental results through a solubility ratio β/α and a viscosity ratio η_u/η_c. It was found that the distribution of the metal into the diluent (β) is about 1.27 and 1.07 times the distribution of the metal into the carrier (α) for iron and manganese, respectively. Also, the viscosity of the complexed carrier (η_c) is about 25 and 160 times the viscosity of the uncomplexed carrier (η_u) for iron and manganese, respectively.

MODEL DEVELOPMENT

Consider a porous carrier-facilitated SLM placed between two finite reservoirs having solute concentrations of C_{b10} and C_{b20}, respectively. The SLM consists of an extracting reagent (i.e., a metal carrier) dissolved in a water-immiscible low dielectric constant organic diluent. The microporous polymeric film made of polypropylene (a hydrophobic material) has a thickness of about 25–50 μm with pore sizes ranging from 0.02 to 1.0 μm.

The following physical and chemical phenomena are assumed to occur during the transport of metal ions across SLMs. First, chemically based effects are distribution mechanisms and solubility effects of a carrier and its diluent (2–4). Second, diffusional effects within the membrane are (a) diffusive effects, viscous effects, and their interactions; and (b) pore size effects. Third, interfacial effects are (a) interfacial reaction effects and (b) concentration polarization effect; that is, the mass transfer resistance at the boundary layer adjacent to each interface.

Equations describing the concentrations of the solute in the supported liquid membrane (SLM), the extracting source phase (ESP), and the stripping sink phase (SSP) are as follows.

SLM:

$$\frac{\partial C}{\partial t} = \mathscr{D}_e \frac{\partial^2 C}{\partial x^2}, \qquad 0 < x < 1 \tag{1}$$

$$t = 0; \qquad C = 0, \qquad 0 < x < 1 \tag{1a}$$

MARCEL DEKKER, INC.
270 Madison Avenue, New York, New York 10016

$$x = 0; \qquad \mathcal{D}_e \frac{\partial C(0, t)}{\partial x} = \frac{(K_1/K_1)C(0, t) - C_{b1}}{(1/K_{m1}) + (1/K_1)}, \qquad t < 0 \quad (1b)$$

$$x = 1; \qquad \mathcal{D}_e \frac{\partial C(1, t)}{\partial x} = \frac{C_{b2} - (K_2/K_2)C(1, t)}{(1/K_{m2}) + (1/K_2)}, \qquad t > 0 \quad (1c)$$

ZSP:

$$V_1 \frac{dC_{b1}}{dt} = A\mathcal{D}_e \frac{\partial C(0, t)}{\partial x} \quad (2)$$

$$t = 0; \qquad C_{b1} = C_{b10} \quad (2a)$$

SSP:

$$V_2 \frac{dC_{b2}}{dt} = -A\mathcal{D}_e \frac{\partial C(1, t)}{\partial x} \quad (3)$$

$$t = 0; \qquad C_{b2} = C_{b20} \quad (3a)$$

where l is the thickness of the membrane, A is the membrane area, V_1 and V_2 are the volumes of the source phase and sink phase, respectively, $C(x, t)$ is the solute concentration within the supported liquid membrane and is defined as the moles per unit membrane volume, and K_j and K_{mj} refer to the interfacial reaction rate constants and the mass transfer coefficients in the extracting side ($j = 1$, $m =$ mass transfer) and the stripping side ($j = 2$), respectively.

For diffusion within the membrane, Fick's law is applicable with the assumption that diffusivity is independent of concentration and spatial coordinates. The flux is defined as the number of moles transported through the membrane per unit total area of the membrane per unit time. It can be written as

$$J = -\mathcal{D}_e \frac{\partial C}{\partial x} \quad (4)$$

Here, $\mathcal{D}_e$ is the effective diffusivity and is defined as

$$\mathcal{D}_e = \frac{D_0 \epsilon' K_r K_p}{\tau'} \quad (5)$$

where D_0 is the free bulk diffusion coefficient for the solute calculated using the Stokes–Einstein equation or the Wilke–Chang equation, ϵ' is the porosity of the membrane, and τ' is the tortuosity factor which takes into account the difference between the effective thickness and the physical thickness. K_r is the fractional reduction in diffusivity caused by pores having a size comparable to the solute molecules. It may be calculated using the following equation (13):

$$K_r = 1 - 2.104\left(\frac{a}{r_e}\right) + 2.09\left(\frac{a}{r_e}\right)^3 - 0.95\left(\frac{a}{r_e}\right)^5 \quad (6)$$

and K_p is the exclusion coefficient equal to $[1 - (a/r_e)]^2$.

The equations can be cast into dimensionless form by defining:

$$y = x/l; \qquad \tau = \mathcal{D}_e t/l^2; \qquad E = C/C_{b10}K_{e1} \quad (7a)$$

$$h = C_{b1}/C_{b10}; \qquad g = C_{b2}/C_{b10}; \qquad \alpha = AlK_{e1}/V_1 \quad (7b)$$

$$\alpha' = AlK_{e1}/V_2; \qquad \beta = K_{e2}/K_{e1}; \qquad \gamma = C_{b20}/C_{b10} \quad (7c)$$

$$B_{i1} = lK_{m1}/\mathcal{D}_e; \qquad B_{i2} = lK_{m2}/\mathcal{D}_e; \qquad N_1 = lK_1/\mathcal{D}_e \quad (7d)$$

$$N_2 = lk_2/\mathcal{D}_e; \qquad \alpha'/\alpha = V_1/V_2; \qquad \tilde{t} = \alpha\tau = \frac{A}{1V_1}K_{e1}\mathcal{D}_e t \quad (7e)$$

$$K_{e1} = K_1/K_1; \qquad K_{e2} = \kappa_2/k_2 \quad (7f)$$

The resulting dimensionless model equations are as follows:

SLM:

$$\frac{\partial E}{\partial \tau} = \frac{\partial^2 E}{\partial y^2}, \qquad 0 < y < 1 \quad (8)$$

$$\tau = 0; \qquad E = 0, \qquad 0 < y < 1 \quad (8a)$$

$$y = 0; \qquad \frac{\partial E(0,\tau)}{\partial y} = \left(\frac{1}{K_{e1}}\right)\frac{E(0,\tau) - h}{(1/B_{i1}) + (1/N_1)}, \qquad \tau > 0 \quad (8b)$$

$$y = 1; \qquad \frac{\partial E(1,\tau)}{\partial y} = \left(\frac{1}{K_{e1}}\right)\frac{g - (1/\beta)E(1,\tau)}{(1/B_{i2}) + (1/N_2)}, \qquad \tau > 0 \quad (8c)$$

ESP:

$$\frac{dh}{d\tau} = \alpha\frac{\partial E(0,\tau)}{\partial y} \quad (9)$$

$$\tau = 0; \qquad h = 1 \quad (9a)$$

SSP:

$$\frac{dg}{d\tau} = -\alpha'\frac{\partial E(1,\tau)}{\partial y} \quad (10)$$

$$\tau = 0; \qquad g = \gamma \quad (10a)$$

The steady-state solution and the transient solution of the system of Eqs. (8)–(10) are summarized in Table 2.

TABLE 2
Solutions for Systems of Equations (8)–(10). Case A: Slow Interfacial Reactions with Aqueous Diffusional Resistance[a]

Region	Steady-state solution	Transient solution
SLM	$C_\infty = \dfrac{V_1C_{b10} + V_2C_{b20}}{(V_1/K_{e1}) + (V_2/K_{e2}) + Al}$	$E = \dfrac{\beta\left(\frac{\alpha'}{\alpha} + \gamma\right)}{\left(1 + \frac{\alpha'}{\alpha}\gamma\right)} + \left\{\dfrac{(1 - \beta\gamma)}{\left(1 + \frac{\alpha'}{\alpha}\beta\right)} - \dfrac{(1 - \beta\gamma)}{\Omega}[y + K_{e1}(B_{i1}^{-1} + N_1^{-1})]\right\} e^{-1/\Omega(1+\alpha'/\alpha\beta)\tilde{t}}$
ESP	$C_{b1\infty} = \dfrac{V_1C_{b10} + V_2C_{b20}}{V_1 + (K_{e1}V_2/K_{e2}) + K_{e1}Al}$	$h = \dfrac{\beta\left(\frac{\alpha'}{\alpha} + \gamma\right)}{\left(1 + \frac{\alpha'}{\alpha}\beta\right)} + \dfrac{(1 - \beta\gamma)}{\left(1 + \frac{\alpha'}{\alpha}\beta\right)} e^{-1/\Omega(1+\alpha'/\alpha\beta)\tilde{t}}$
SSP	$C_{b2\infty} = \dfrac{V_1C_{b10} + V_2C_{b20}}{V_2 + (K_{e2}V_1/K_{e1}) + K_{e2}Al}$	$g = \dfrac{\left(\frac{\alpha'}{\alpha} + \gamma\right)}{\left(1 + \frac{\alpha'}{\alpha}\beta\right)} - \dfrac{\frac{\alpha'}{\alpha}(1 - \beta\gamma)}{\left(1 + \frac{\alpha'}{\alpha}\beta\right)} e^{-1/\Omega(1+\alpha'/\alpha\beta)\tilde{t}}$

[a] $\tilde{t}$ = slow time = $\alpha\tau$. $\Omega = 1 + K_{e1}(B_{i1}^{-1} + N_1^{-1}) + K_{e2}(B_{i2}^{-1} + N_2^{-1})$.

MARCEL DEKKER, INC.
270 Madison Avenue, New York, New York 10016

Special Case 1

Fast Interfacial Reactions with Negligible Aqueous Diffusional Resistance

When the interfacial chemical reactions are fast (i.e., $K_1 \to \infty$ and $K_2 \to \infty$) and the aqueous diffusional resistances are negligible (i.e., $k_{m1} \to \infty$ and $k_{m2} \to \infty$), the boundary conditions (Eqs. 1b and 1c) become

$$x = 0; \qquad C = K_{e1} C_{b1} \tag{11}$$

$$x = 1; \qquad C = K_{e2} C_{b2} \tag{11a}$$

Their corresponding nondimensional forms are

$$y = 0; \qquad E = h \tag{11b}$$

$$y = 1; \qquad E = \beta g \tag{11c}$$

The steady-state solution of the resulting system of equations is the same for all cases and was shown earlier in Table 2. The results of the transient solution of this system of equations are shown below. The key

$$E = h - (h - \beta g)y \tag{12}$$

$$h = \frac{\beta\left(\frac{\alpha'}{\alpha} + \gamma\right)}{\left(1 + \frac{\alpha'}{\alpha}\beta\right)} + \frac{(1 - \beta\gamma)}{\left(1 + \frac{\alpha'}{\alpha}\beta\right)} e^{-(1+\alpha'/\alpha\beta)\tilde{t}} \tag{13}$$

$$g = \frac{\left(\frac{\alpha'}{\alpha} + \gamma\right)}{\left(1 + \frac{\alpha'}{\alpha}\beta\right)} - \frac{\frac{\alpha'}{\alpha}(1 - \beta\gamma)}{\left(1 + \frac{\alpha'}{\alpha}\beta\right)} e^{-(1+\alpha'/\alpha\beta)\tilde{t}} \tag{14}$$

RESULTS AND DISCUSSIONS

Concentration Profiles within the Membrane Matrix

Figure 3 shows the theoretical linear concentration profiles within the membrane matrix for a case governed by a slow reaction and mass transfer resistance in the boundary layers adjacent to the membrane. It can be seen that the concentration profile is sharp in the beginning of the process and approaches a steady-state after long times (in this case after 100 hours). The assumed parameters characterizing the system for these profiles are: $K_{e1} = 10$, $K_{e2} = 0.1$, $B_{i1} = 50$, $B_{i2} = 50$, $N_1 = 7.15$, $N_2 = 13.0$, $A = 25\ cm^2$, $l = 0.0025$ cm, $V_1 = 500\ cm^3$, $V_2 = 500\ cm^3$, $C_{10} = 0.001$ M, $C_{b20} = 0.0$, and $\mathcal{D}_e =$

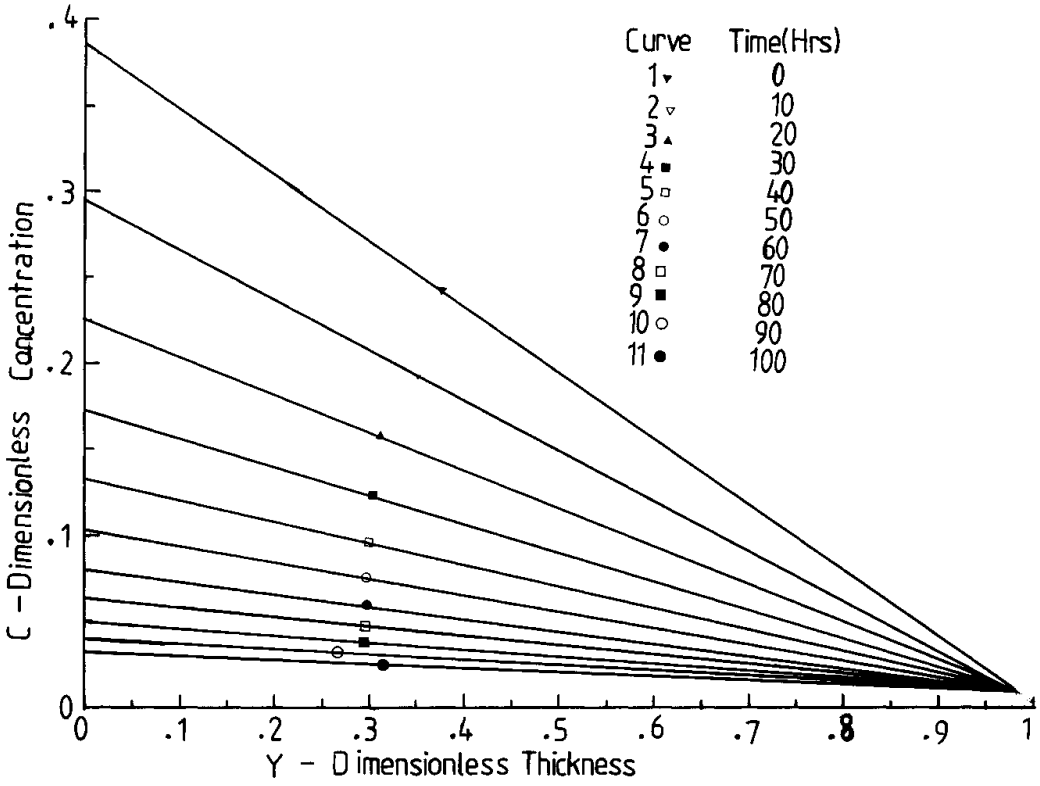

FIG. 3 Concentration profiles throughout the membrane matrix after 0 to 100 hours time. $K_{e1} = 10$, $K_{e2} = 0.1$, $B_{i1} = 50$, $B_{i2} = 50$, $N_1 = 7.15$, $N_2 = 13.0$, $A = 25$ cm^2, $l = 0.0025$, $V_1 = 500$ cm^3, $V_2 = 500$ cm^3, $C_{b10} = 0.001$M, $C_{b20} = 0.0$, and $\mathcal{D}_e = 1 \times 10^{-7}$ cm^2/s.

1×10^{-7} cm^2/s. Note that the intramembrane concentration is linear. This is the direct result of the QSSH (i.e., the holdup term for a metal ion in the membrane is ignored). This has been justified by using a perturbation analysis in which the parameters α and α' are assumed very small numbers ($\alpha, \alpha' \ll 1$) and their ratio is assumed to be of the order of unity. The model solutions are reasonable and can be used for practical purposes. These concentration gradients constitute the major driving force responsible for the transport of metal ions between the source reservoir and the sink reservoir, even when the two reservoirs have equal metal concentrations (i.e., active transport).

Time Scale Analysis

From the model equations (Table 2) developed for the general case (i.e., slow interfacial reactions with aqueous diffusional resistance), the time scale equation could be written as

$$t = \frac{l[1 + K_{e1}(B_{i1}^{-1} + N_1^{-1}) + K_{e2}(B_{i2}^{-1} + N_2^{-1})]}{(A/V_1)K_{e1}\mathcal{D}_e\left(1 + \frac{V_1K_{e2}}{V_2K_{e1}}\right)} \quad (15)$$

By looking at the time scale equation, the following effects can be studied.

Effect of Membrane Thickness l on the Process

It is found that as one increases the membrane thickness, the time scale will increase linearly, causing a decrease in the flux. Figure 4 shows the effect of membrane thickness on the time scale. An increase of membrane thickness by a factor of 5 will increase the time scale by a factor of 5. Babcock et al. (14, 15) looked at the effect of reciprocal membrane thickness on uranium flux for two experiments with feed solutions with different pH values (i.e., pH 1 and 3). In order to eliminate concentration polarization effects, stirring rates of 600 rpm were used. The results show that the plot is linear, indicating

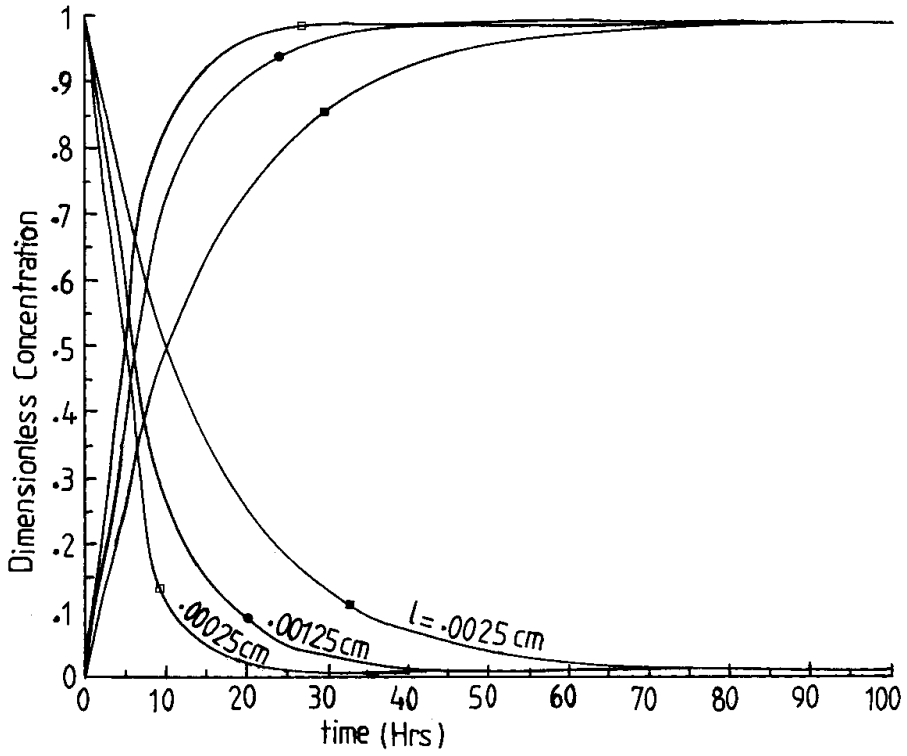

FIG. 4 Effect of membrane thickness on the concentration profiles of the extraction side and the strip side. $l = 0.00025$, 0.00125, and 0.0025 cm. $K_{d1} = 10$, $K_{d2} = 0.1$, $B_{i1} = 50$, $B_{i2} = 50$, $N_1 = 7.15$, $N_2 = 13$, $A = 25$ cm^2, $V_1 = 100$ cm, $V_2 = 100$ cm^3, $C_{b10} = 1.0$ M, $C_{b20} = 0.0$, and $\mathcal{D}_e = 5 \times 10^{-8}$ cm^2/s.

diffusion-limited flux even with the thinnest membranes. At a higher pH (i.e., pH 3), the flux reaches a limiting value with thinner membranes because it was found that the rate of the interfacial reaction is proportional to the hydrogen ion concentration raised to the fourth power; that is, the flux is kinetically controlled.

Effect of Available Membrane Surface Area per Unit Volume of Reactor (A/V_1) on the Process

It is found that as one increases the membrane surface area per unit volume available for transporting the desired species, the time scale decreases linearly, causing an increase in the flux. Marr and Kopp (16) reported this ratio (A/V_1) to be equal to about 10^3 to 3×10^3 m^2/m^3 in liquid emulsion membranes, 10^3 m^2/m^3 for hollow fiber SLM, 100–200 m^2/m^3 for flat SLM, and about 50 m^2/m^3 for tubular membrane modules. It is therefore very attractive to work with either liquid emulsion membranes or with hollow fiber SLM because of their high packaging densities. Figure 5 shows the effect of (A/V_1) on the

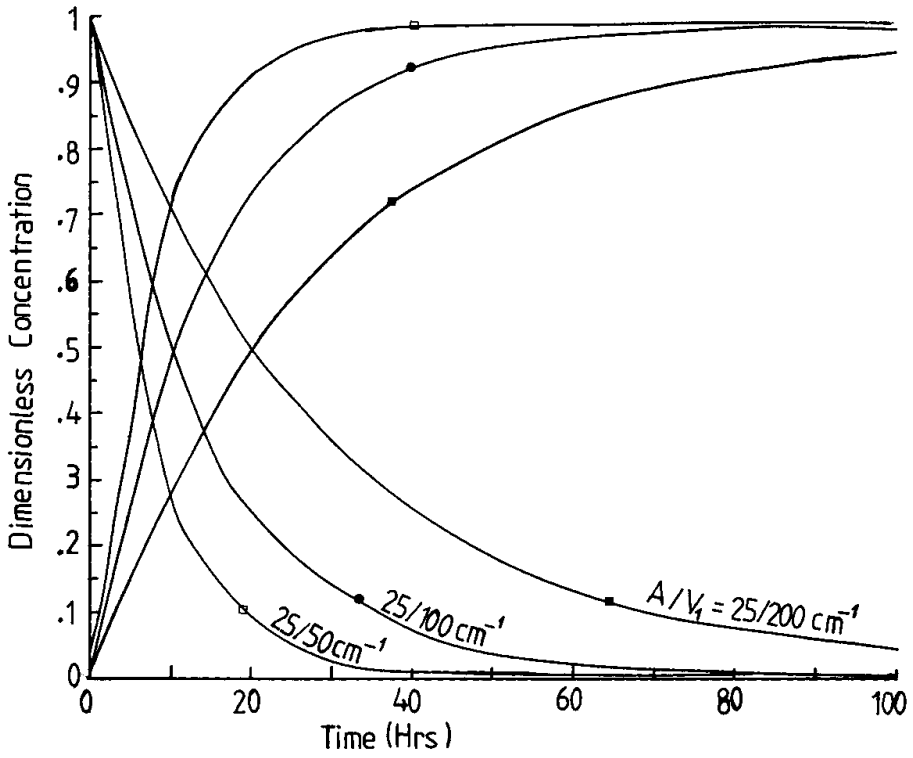

FIG. 5 Effect of the ratio A/V_1 on the concentration profiles of the extraction side and the strip side. A/V_1 = 25/200, 25/100, and 25/50 cm. K_{e1} = 100, K_{e2} = 0.1, B_{i1} = 50, B_{i2} = 50, N_1 = 7.15, N_2 = 13, A = 25 cm^2, V_2 = 100 cm^3, C_{b10} = 1 M, C_{b20} = 0, and $\mathcal{D}_e$ = 5×10^{-8} cm^2/s.

MARCEL DEKKER, INC.
270 Madison Avenue, New York, New York 10016

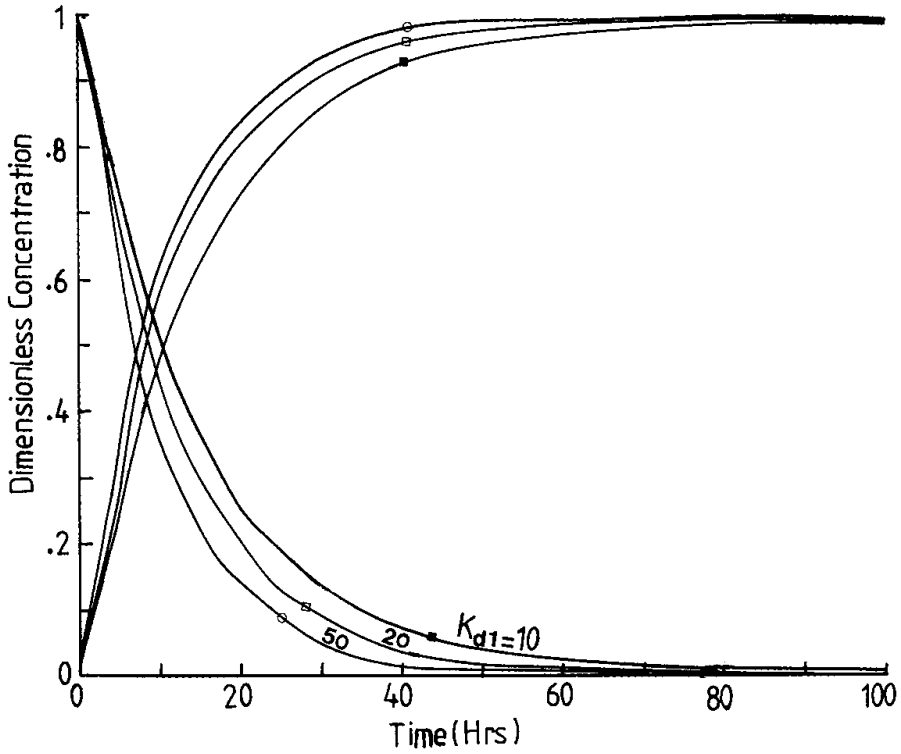

FIG. 6 Effect of K_{e1} on the concentration profiles of the extraction side and the strip side. K_{e1} = 10, 20, and 50. K_{e2} = 0.1, B_{i1} = 50, B_{i2} = 50, N_1 = 7.15, N_2 = 13, A = 25 cm^2, V_1 = 100 cm^3, V_2 = 100 cm^3, C_{b10} = 1.0 M, C_{b20} = 0.0, and $\mathcal{D}_e$ = 5 $\times$ 10^{-8} cm^2/s.

time scale. An increase of (A/V_1) by a factor of 2 will decrease the time scale by a factor of 2.

Effect of the Effective Equilibrium Constant at the Extracting Interface (K_{e1}) on the Process

It is found that as one increases the effective equilibrium constant at the extracting interface, the time scale will decrease linearly, causing an increase in the flux. Figure 6 shows the effect of K_{e1} on the time scale. An increase of K_{e1} by a factor of 2 will decrease the time scale by a factor of 2. The functional behavior of K_{e1} for the case of divalent metals can be derived (4) as

$$K_{e1} = \frac{(MG_2)_{O1}}{(M^{2+})_{O1}} \frac{(H^+)^2_{A1}}{(HG)^2_{O1}} \tag{16}$$

(for an acidic carrier counter transport mechanism)

$$K_{e1} = \frac{(M1_2 \cdot 2TX)_{O1}}{(M^{2+})_{O1}} (TX)_{O1}^{-2} (l^-)_{A1}^{-2} \quad (17)$$

(for a neutral carrier cotransport mechanism)

where the subscripts O and A refer to the organic and aqueous phases, respectively. The subscript 1 refers to the extraction side. H^+ and l^- refer to the coupling ion which represents the hydrogen ion in the case of the countertransport mechanism and the ligand ion in the case of the cotransport mechanism. HG and TX represent the acidic carrier and the neutral carrier, respectively.

Chemically based effects other than the distribution mechanism effect described above include the solubility effect. The distribution of a species from an aqueous phase into an organic phase depends significantly on the difference between its hydration energies within the aqueous phase and solvation energies in the organic phase composed of the diluent and its carrier. The distributed metal concentration in the liquid membrane phase can be written as

$$M^* = M[\alpha^* \bar{x} + \beta^*(1 - \bar{x})] \quad (18)$$

where M and M* represent the metal concentrations in the aqueous and liquid membranes phases, respectively. α^* is the distribution coefficient at 100% carrier ($\bar{x} = 1$) and β^* is the distribution coefficient at 0% carrier. A detailed discussion of this effect is in our earlier paper (2).

Effect of the Effective Diffusivity on the Process

It was found that as the effective diffusivity increases, the time scale of the process decrease, linearly, causing an increase in the flux. Figure 7 shows that increasing the effective diffusivity by a factor of 2 will decrease the time scale by a factor of 2. The effective diffusivity can be estimated from the Stokes–Einstein equation with some modifications as follows:

$$\mathcal{D}_e = D_0 \frac{\epsilon' K_r K_p}{\tau'} = \frac{kT\epsilon' K_r K_p}{6\pi r \eta \tau'} \quad (19)$$

Several effects related to the effective diffusivity will now be discussed.

1. *Effect of viscosity on diffusivity*. There is a negative effect of viscosity on diffusivity. As the viscosity of the organic phase increases with increasing carrier concentration, the effective diffusivity of the metal carrier complex decreases. If the viscosity of the complexed carriers and the uncomplexed carriers are denoted as η_c and η_u, respectively, then the viscosity of the mixture may be calculated as follows:

$$\eta = \eta_c \bar{x} + \eta_u(1 - \bar{x}) \quad (20)$$

MARCEL DEKKER, INC.
270 Madison Avenue, New York, New York 10016

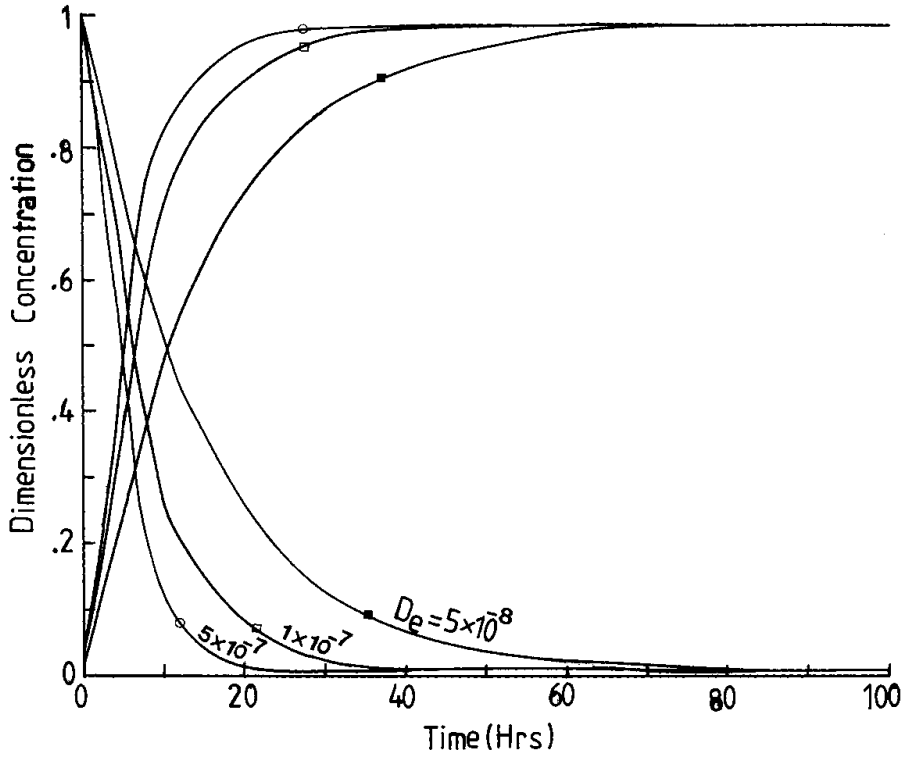

FIG. 7 Effect of $\mathcal{D}_e$ on the concentration profiles of the extraction side and the strip side. $\mathcal{D}_e = 5 \times 10^{-8}$, 1×10^{-7}, and 5×10^{-7} cm^2/s. $K_{e1} = 10$, $K_{e2} = 0.1$, $B_{i1} = 50$, $B_{i2} = 50$, $N_1 = 7.15$, $N_2 = 13$, $A = 25$ cm^2, $V_1 = 100$ cm^3, $V_2 = 100$ cm^3, $C_{b10} = 1.0$, and $C_{b20} = 0.0$.

where $\bar{x}$ is the concentration of the carrier. A detailed discussion of this effect is in our earlier paper (3).

2. *Pore size effects*. Beck et al. (13) found that there can be a twofold flux reduction due to hindered diffusion when the radius of the permeant is about 15% of the pore radius.
3. *Other effects*. It was found that as the temperature increases, the effective diffusivity increases, causing a linear increase in the flux (17). An increase in porosity increases the effective diffusivity, causing an increase in the flux. Akiba and Kanno (18) reported the use of a porous polytetrafluoroethylene film (Fluoropore FP-045m Sumitomo Electric Ind.) with a thickness of 80 μm, a porosity of 74%, and an average pore size of 0.45 μm. This is compared to Celgard 2500 with a thickness of 25 μm, a porosity of 45%, and an average pore size of 0.04 μm. An inverse behavior of the tortuosity factor is expected because the membrane pores are very tortuous.

Interfacial Effects (Ω)

These effects include the following.

1. *Concentration polarization effects*. At low stirring rates (B_{i1} and B_{i2} are very small), the stagnant boundary layer adjacent to the membrane interface is relatively thick. This will tend to create a large resistance to the transfer process, thus reducing the flux. As the stirring rate is increased, the flux will increase up to a maximum limiting value, after which further increases in the stirring rate have no effect. Figure 8 shows the effect of the Biot number in the extracting side (B_{i1}) on the time scale. Babcock et al. (14, 15) looked at the effect of stirring rate on uranium flux for two experiments with feed solutions of different pH values (that is, pH 1 and 3). They found that the external mass transfer resistance at the extracting side becomes significant when the stirring rate is less than 150 rpm. On the other hand, they found that the external mass transfer resistance is negligible at the stripping side. This can be explained in two

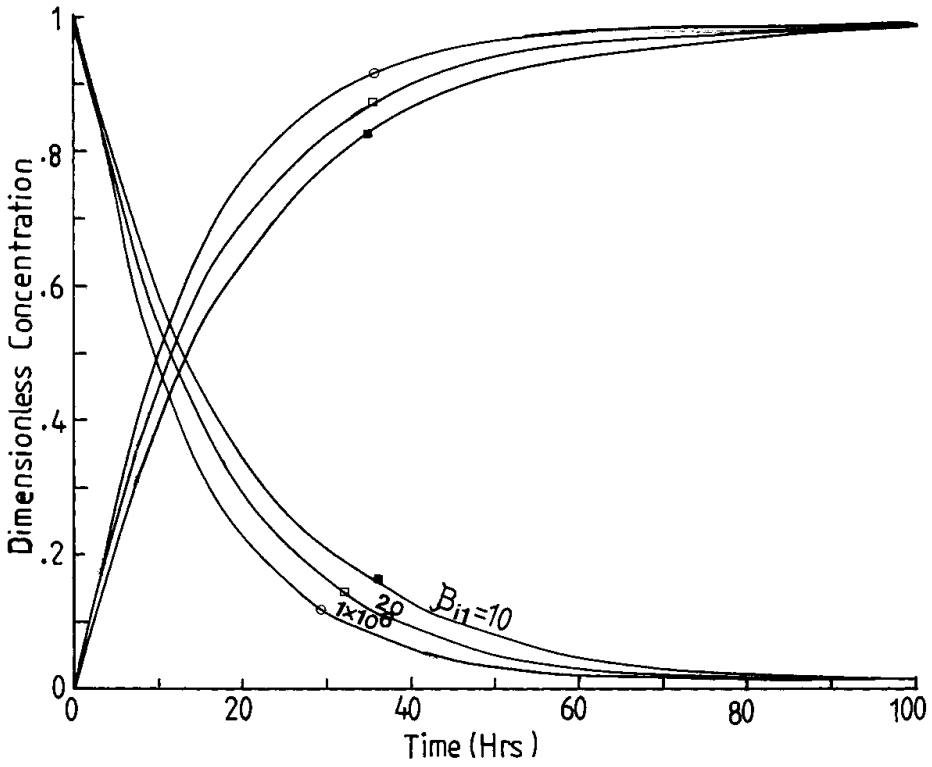

FIG. 8 Effect of B_{i1} on the concentration profiles of the extraction side and the strip side. B_{i1} = 10, 20, and 1×10^6. K_{e1} = 10, K_{e2} = 0.1, B_{i2} = 50, N_1 = 7.15, N_2 = 13, A = 25 cm^2, V_1 = 100 cm^3, V_2 = 100 cm^3, C_{b10} = 1.0, C_{b20} = 0.0, and $\mathcal{D}_e = 5 \times 10^{-8}$ cm^2/s.

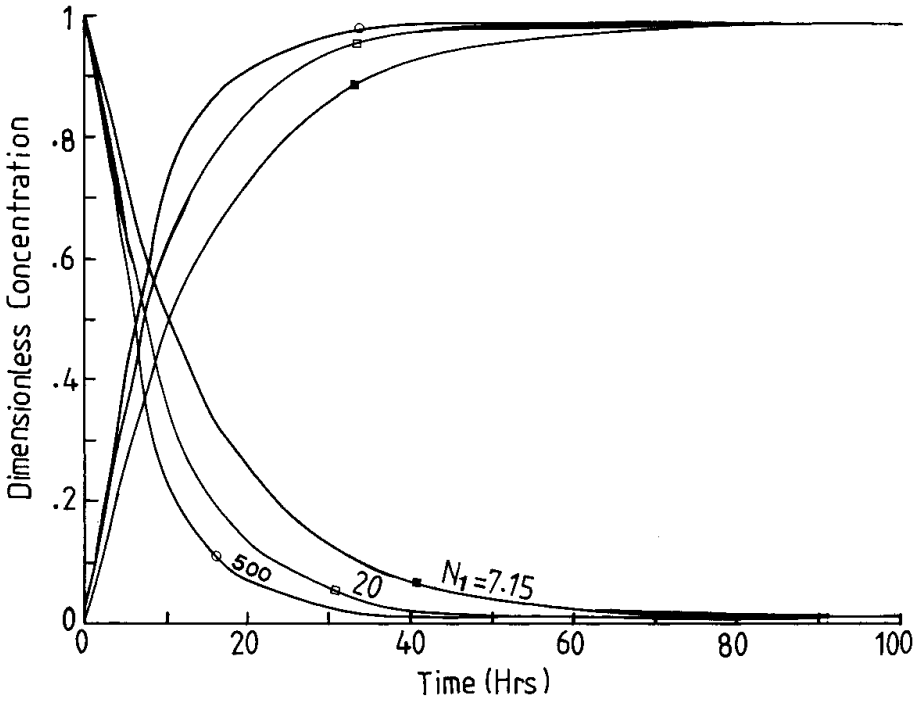

FIG. 9 Effect of N_1 on the concentration profiles of the extraction side and the strip side. N_1 = 7.15, 20, and 500. K_{e1} = 10, K_{e2} = 0.1, B_{i1} = 50, B_{i2} = 50, N_2 = 13, A = 25 cm^2, V_1 = 100 cm^3, V_2 = 100 cm^3, C_{b10} = 1.0 M, C_{b20} = 0.0, and $\mathcal{D}_e = 5 \times 10^{-8}$ cm^2/s.

ways: mathematically, B_{i2}^{-1} is multiplied by a very small number (K_{e2}), therefore its contribution is negligible. Physically, a small value of K_{e2} results in a small value of K_{d2}, which gives a high distribution of the metal species from the organic liquid membrane phase into the stripping aqueous phase. If K_{e1} and K_{e2} are comparable, B_{i2} will exhibit a similar influence as B_{i1} shown in Fig. 8.

2. *Effect of interfacial reaction rates*. When the interfacial reaction rates control the process (that is, the rates of the reaction are very slow and N_1 and N_2 are very small), the time scale is lengthened, which causes the flux to decrease. Figure 9 shows the effect of the rate of reaction to diffusion in the extracting interface (N_1) on the time scale. Danesi et al. (7) reported that the system copper–water–LIX 64N to be controlled by the kinetics of the interfacial reactions. The interfacial chemical reaction rates (K_1 and K_2) were reported to equal 2.86×10^{-4} and 5.2×10^{-4} cm/s, respectively. They also reported that the process is controlled by the boundary layer resistance at lower stirring rates such as 60 rpm. The effect of the rate of reaction to diffusion in the stripping side (N_2) was found to be negligible. This can be explained in two ways: mathemati-

cally, N_2^{-1} is multiplied by a vary small number (K_{e2}), therefore its contribution is negligible. Physically, N_1 and N_2 are related to the equilibrium constants of the reactions K_{e1} and K_{e2} and hence to the distribution coefficients K_{d1} and K_{d2}. For very fast reactions in the forward direction from the organic phase to the aqueous phase (N_2 is very small because it is defined in the backward direction from the aqueous to the organic phase), K_{e2} is very small and K_{d2} is also very small. For comparable K_{e1} and K_{e2}, N_2 will exhibit a similar behavior as N_1 shown in Fig. 9.

Effect of the Effective Equilibrium Constant in the Stripping Side (K_{e2})

It was found that as the effective equilibrium constant decreases at the stripping interface, the time scale will decrease, causing an increase in the flux. Figure 10 shows the effect of K_{e2} on the time scale. Initially, K_{e2} has

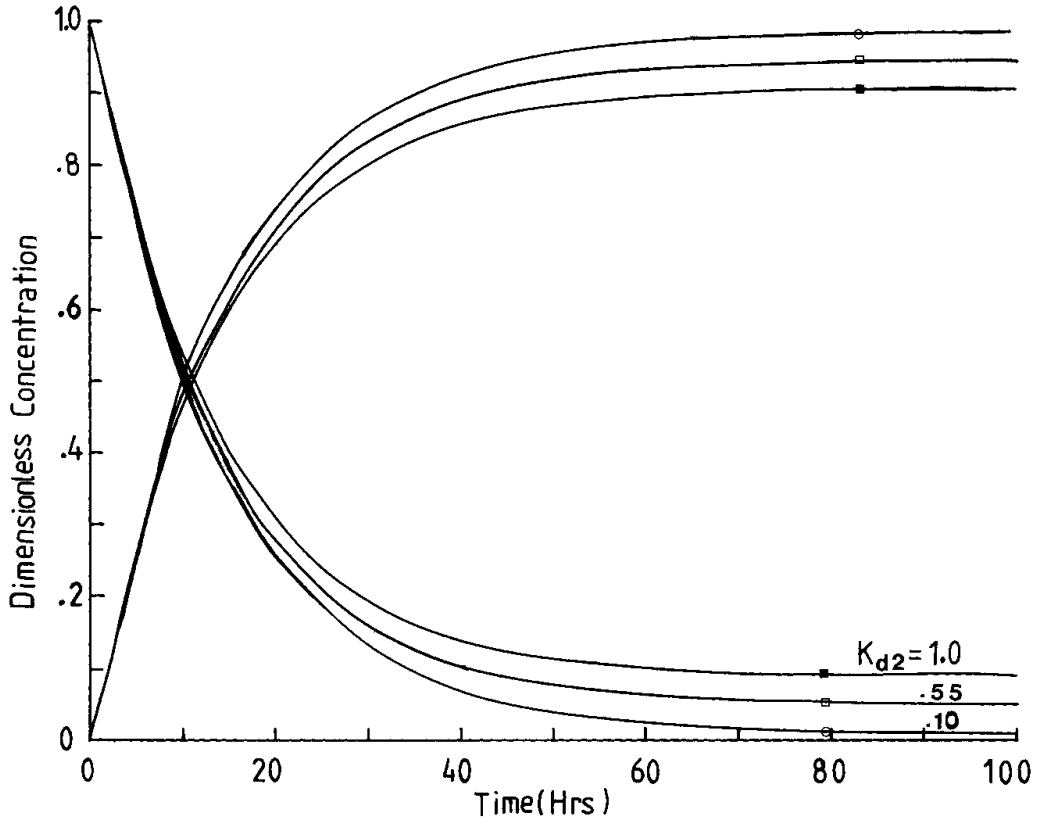

FIG. 10 Effect of K_{e2} on the concentration profiles of the extraction side and the strip side. $K_{e2} = 1.0$, 0.55, and 0.10. $K_{e1} = 10$, $B_{i1} = 50$, $B_{i2} = 50$, $N_1 = 7.15$, $N_2 = 13.0$, $A = 25$ cm^2, $V_1 = 100$ cm^3, $V_2 = 100$ cm^3, $C_{b10} = 1.0$ M, $C_{b20} = 0.0$, and $\mathcal{D}_e = 5 \times 10^{-8}$ cm^2/s.

no effect on the process (i.e., up to 10 hours); however, at a later time the effect of K_{e2} becomes more pronounced. This is caused by the more rapid accumulation of species in the membrane and their rapid depletion at lower K_{e2} values. The functional behavior of K_{e2} for the case of divalent metals can be derived (4) as

$$K_{e2} = \frac{(MG_2)_{O2}}{(M^{2+})_{O2}} \frac{[HG]^2_{O2}}{[H^+]^2_{A2}} \tag{21}$$

for an acidic extractant carrier (countertransport mechanism)

$$K_{e2} = \frac{(Ml_2 \cdot 2TX)_{O2}}{(M^{2+})_{O2}} (TX)^2_{O2} (l^-)^2_{A2} \tag{22}$$

for a neutral extractant carrier (cotransport mechanism)

where the subscript 2 refers to the strip side. A decrease of K_{e2} by a factor of do would decrease the steady-state dimensionless concentration by a factor of 10. The steady-state dimensionless concentration in Fig. 10 can be corre-

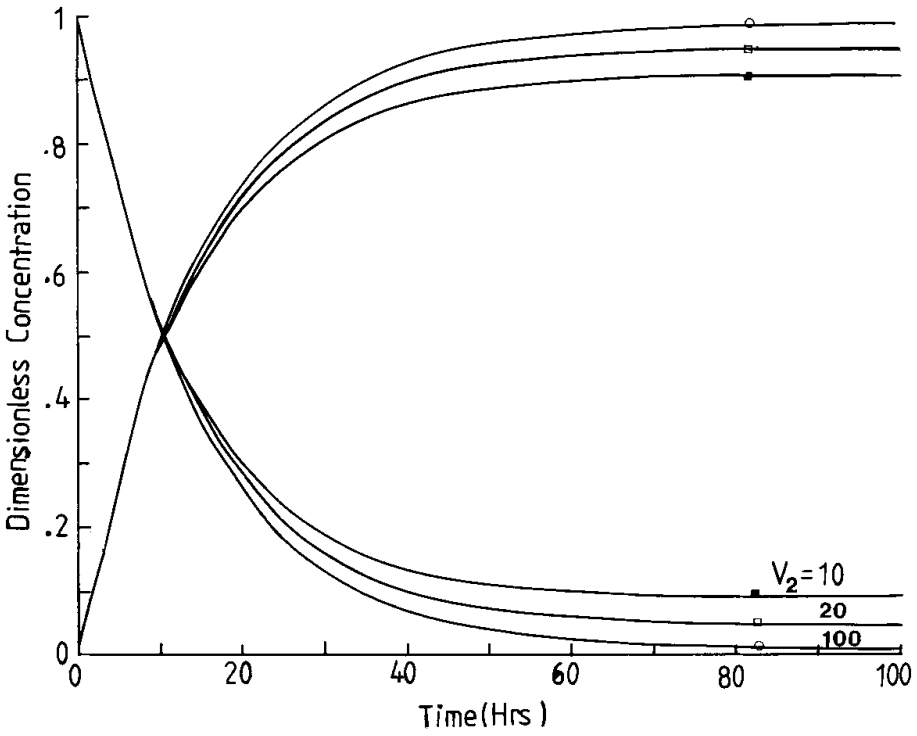

FIG. 11 Effect of V_2 on the extraction profiles of the extraction side and the strip side. V_2 = 10, 20, and 100 cm^3. K_{e1} = 10, K_{e2} = 0.1, B_{i1} = 50, B_{i2} = 50, N_1 = 7.15, N_2 = 13, A = 25 cm^2, V_1 = 100 cm^3, C_{b10} = 1.0 M, C_{b20} = 0.0, and $\mathscr{D}_e = 5 \times 10^{-8}$ cm^2/s.

lated to K_{e2} by the following relation:

$$h_\infty = 0.1K_{e2} \tag{23}$$

Effect of the Sink Volume (V_2)

It was found that as the sink volume V_2 increases, the time scale will decrease, causing an increase in the flux. Figure 11 shows the effect of V_2 on the time scale of the process. Akiba et al. (18) stated that a high volume ratio V_1/V_2 is desirable to concentrate uranium from dilute solutions. However, a large volume ratio is not always desirable from the kinetic standpoint, which agrees with our finding. An increase of V_2^{-1} by a factor of 10, would increase the steady-state dimensionless concentration by a factor of 10. The steady-state dimensionless concentration (h;ii) in Fig. 11 can be correlated to V_2^{-1} by the relation

$$h_\infty = 1/V_2 \tag{24}$$

CONCLUSION

The first part of this work reports the mathematical modeling of the mass transfer rates of metal ions across supported liquid membranes. The results presented in this part are compared directly to experimental data which will be reported in Part II of this work. The model equations were solved using Laplace transform techniques utilizing a slow time concept and a pseudo steady-state assumption. The model was found to be a very useful design equation. The magnitude of the mass transfer resistance (14, 15) and the rate of the interfacial chemical reactions (19) can be estimated by conducting proper experiments. The magnitude of the effective diffusivity can also be calculated by using the Wilke–Chang equation or Stokes–Einstein equation. Through the use of a nonlinear regression technique like the Marquardt nonlinear regression package, useful parameters can be extracted from the model (such as the distribution coefficients in either reservoir, the Biot number, the rates of interfacial chemical reactions, and the effective diffusivities) which can be checked with experimental values and used for design purposes. The theoretical model was found to simulate experimental results best by using a three-parameter model. Also, the model was found to simulate active transport data quite closely. Time-scale analysis clearly showed the effects of different parameters on the transfer rates.

NOTATION

a	intercept of linear regression correlation
A	membrane area (cm^2)

A_1	first nonlinear regression parameter, $\dfrac{\dfrac{V_1}{V_2} + \dfrac{B_{b20}}{C_{b10}}}{1 + \dfrac{V_1}{V_2}\dfrac{K_{e2}}{K_{e1}}}$
A_2	second nonlinear regression parameter, $\dfrac{\dfrac{V_1}{V_2}\left(1 - \dfrac{K_{e2}}{K_{e1}}\dfrac{C_{b20}}{C_{b10}}\right)}{1 + \dfrac{V_1}{V_2}\dfrac{K_{e2}}{K_{e1}}}$
A_3	third nonlinear regression parameter, $\left(1 + \dfrac{V_1}{V_2}\dfrac{K_{e2}}{K_{e1}}\right)\dfrac{A}{V_1 l}K_{e1}\mathscr{D}_e$
b	slope of linear regression correlation
B2EHHP	bis(2-ethylhexyl) hydrogen phosphate
$\mathscr{C}$	denotes the carrier
C	concentration within membrane (moles per unit volume of membrane)
C_{b1}	bulk concentration in extraction reservoir (moles per unit volume of reservoir)
C_{b2}	bulk concentration in strip reservoir (moles per unit volume of reservoir)
C;ii	steady-state concentration within membrane
$C_{b1\infty}$	steady-state concentration within extraction reservoir, C_∞/K_{e1}
$C_{b2\infty}$	steady-state concentration within strip reservoir, C_∞/K_{e2}
$\mathscr{D}_M$	diffusion coefficient of the metal species
$\mathscr{D}_R$	diffusion coefficient of the metal–carrier complex
$\mathscr{D}_e$	effective diffusivity, $\epsilon' k_r k_p/\tau'$ (cm^2/s)
$\mathscr{D}_0$	free bulk diffusion coefficient
$\mathscr{D}_e$	average effective diffusivity (cm^2/s)
E	dimensionless concentration within membrane, $C/C_{b10}k_{e1}$
ESP	extraction source phase
F	$\sum_{i=1}^{N}(y_i - \bar{y}_i)^2$
$F(s)$	Laplace function
$g(s)$	Laplace function
g	dimensionless concentration in strip reservoir
g;ii	steady-state dimensionless concentration in strip reservoir
h	dimensionless concentration in strip reservoir
$\bar{h}$	dimensionless concentration in strip reservoir in Laplace domain
(HX)	denotes an acidic extractant carrier concentration
(H^+)	denotes hydrogen ion concentration
J	membrane flux, $-\mathscr{D}_e\dfrac{\partial C}{\partial x}$

MARCEL DEKKER, INC.
270 Madison Avenue, New York, New York 10016

K_{d1}	distribution coefficient in extraction interface
K_{d2}	distribution coefficient in strip interface
K_{m1}	mass transfer coefficient in extraction boundary layer
K_{m2}	mass transfer coefficient in strip boundary layer
K_{e1}	equilibrium constant of interfacial chemical reaction in extraction phase
K_{e2}	equilibrium constant of interfacial chemical reaction in strip phase
l	membrane thickness, cm
l^-	extraction phase complexing ligand anion
L	extraction phase complexing ligand
M	metal species
M*	distributed metal species into liquid membrane
ML_N	aqueous metal–ligand complexes
P	permeability coefficient, J/C_{b10} (cm/s)
R	metal–carrier complex
r_e	pore radius
R^2	multiple correlation coefficient
SLM	supported liquid membrane
SSP	sink strip phase
S	Laplace transform dummy operator
t	real time
(TX)	denotes a neutral extractant carrier concentration
t	slow time ($\alpha\tau$)
T	absolute temperature
V_1	extraction reservoir volume (cm^3)
V_2	strip reservoir volume (cm^3)
w	independent variable in nonlinear regression model equation
x	spatial coordinate
$\bar{x}$	carrier concentration
y	dimensionless coordinate, x/l
y_i	experimental data points estimates
$\bar{y}_i$	theoretical data points estimates
Z	dependent variable in nonlinear regression model equation

Greek Letters

α	AlK_{e1}/V_1
α'	AlK_{e1}/V_2
α'/α	V_1/V_2
α^*	the distribution coefficient in a pure carrier
β^*	the distribution coefficient in a pure diluent

MARCEL DEKKER, INC.
270 Madison Avenue, New York, New York 10016

β	K_{e2}/K_{e1}
B_{i1}	$lK_{m1}/\mathcal{D}_e$
B_{i2}	$lK_{m2}/\mathcal{D}_e$
γ	C_{b20}/C_{b10}
δ_a	aqueous boundary layer thickness
δ_o	organic liquid membrane thickness
ϵ'	porosity of the membrane
η	viscosity of the organic solution
η_u	viscosity of the uncomplexed organic solution
η_c	viscosity of the complexed organic solution
K_1	extraction interfacial chemical reaction rate constant
K_2	stripping interfacial chemical reaction rate constant
K_r	fractional reduction of diffusivity of nonabsorbed solute with pores, $[1 - (a/r_e)]^2$
K_p	exclusion coefficient, $1 - 2.104\,\frac{a}{r_e} + 2.09\left(\frac{a}{r_e}\right)^3 + 0.95\left(\frac{a}{r_e}\right)^5$
K_{i1}	overall formation constants of the metal–ligand aqueous species
τ'	tortuosity of the membrane pores
τ	$\mathcal{D}_e t/l^2$
N_1	$lK_1/\mathcal{D}_e$
N_2	$lK_2/\mathcal{D}_e$
Ω	$1 + K_{e1}(B_{i1}^{-1} + N_1^{-1}) + K_{e2}(B_{i2}^{-1} + \eta_2^{-1})$

Subscripts

0	initial concentration as C_{b10}
1	denotes extraction phase
2	denotes strip phase
A1	denotes aqueous extraction phase
A2	denotes aqueous strip phase
M	denotes metal species M
N	denotes metal species N
O1	denotes organic extraction interface
O2	denotes organic strip interface
Th	thorium
U	uranium

Superscripts

I	denotes first parameter evaluation techniques

MARCEL DEKKER, INC.
270 Madison Avenue, New York, New York 10016

II	denotes second parameter evaluation technique
M	denotes metal species M
N	denotes metal species N
Th	thorium metal species
U	uranium metal species

REFERENCES

1. P. R. Danesi, ''Separation of Metal Species by Supported Liquid Membranes,'' *Sep. Sci. Technol.*, *19*, 857–894 (1984–85).
2. A. A. Elhassadi and D. D. Do, ''Effects of a Carrier and Its Diluent on the Transport of Metals across Supported Liquid Membranes (SLM). I. Solubility Mechanism,'' *Ibid.*, *21*(3), 267–283 (1986).
3. A. A. Elhassadi and D. D. Do, ''Effects of a Carrier and Its Diluent on the Transport of Metals across Supported Liquid Membranes (SLM). II. Viscosity Effect,'' *Ibid.*, *21*(3), 285–297 (1986).
4. A. A. Elhassadi, ''Fundamental Studies of Separation of Metal Ions Using Supported Liquid Membranes—Selective Separation of Uranium and Thorium,'' Ph.D. Thesis, University of Queensland, St. Lucia, Queensland, 1986.
5. I. Komasawa, T. Otake, and A. Yamada, ''Equilibrium Studies of Copper Extraction from Sulfate Media with Hydroxomic Extractant,'' *J. Chem. Eng. Jpn.*, *13*, 130–136 (1980).
6. K. H. Lee, D. F. Evans, and E. L. Cussler, ''Selective Copper Recovery with Two Types of Liquid Membranes,'' *AIChE J.*, *24*, 860–868 (1978).
7. P. R. Danesi, P. Horwitz, G. F. Vandergrift, and R. Chiarizia, ''Mass Transfer Rate through Liquid Membranes: Interfacial Chemical Reactions and Diffusion as Simultaneous Permeability Controlling Factors,'' *Sep. Sci. Technol.*, *16*, 201–211 (1981).
8. A. G. Kopp, R. J. Marr, and F. E. Moser, ''A New Concept for Mass Transfer in Liquid Surfactant Membranes without Carriers and with Carriers That Pump,'' *Inst. Chem. Eng. Symp. Ser.*, *54*, 279–290 (1978).
9. S. A. Netke and V. G. Pangaker, ''Extraction of Naphthenic Acid from Kerosene Using Porous and Nonporous Polymeric Membranes,'' *Sep. Sci. Technol.*, *31*(1), 63–76 (1996).
10. R. S. Juang and H. L. Chang, ''A Mechanistic Study of Uphill Transport of Metal Ions through Countertransport SLM,'' *Ibid*, *31*(3), 365–379 (1996).
11. A. M. Darbi, ''Transport of Iron across SLM,'' M.S. Thesis, University of Garyounis, Benghazi, Libya, 1994.
12. N. M. Hassan, ''Transport of Manganese across SLM,'' M.S. Thesis, University of Garyounis, Benghazi, Libya, 1995.
13. R. E. Beck and J. S. Schultz, ''Hindrance of Solute Diffusion within Membranes as Measured with Microporous Membranes of Known Pore Geometry,'' *Biochim. Biophys. Acta*, pp. 255–273 (1972).
14. W. C. Babcock, R. W. Baker, E. D. Lachapelle, and K. L. Smith, ''Coupled Transport Membranes. II. The Mechanism of Uranium Transport with a Tertiary Amine,'' *J. Membr. Sci.*, *7*, 71–87 (1980).
15. W. C. Babcock, R. W. Baker, E. D. Lachapelle, and K. L. Smith, ''Coupled Transport Membranes. III. The Rate Limiting Step in Uranium Transport with a Tertiary Amine,'' *Ibid.*, *7*, 89–100 (1980).
16. R. Marr and A. Kopp, ''Liquid Membrane Technology, a Survey of Phenomena, Mechanisms, and Models,'' *Int. Chem. Eng.*, *22*, 44–60 (1982).

MARCEL DEKKER, INC.
270 Madison Avenue, New York, New York 10016

17. R. W. Baker, M. E. Tuttle, D. J. Kelly, and H. K. Londsdale, ''Coupled Transport Membranes. I. Copper Separations,'' *J. Membr. Sci., 2*, 213–233 (1977).
18. K. Akiba and T. Kanno, ''Transport of Uranium(VI) through a Supported Liquid Membrane Containing LIX 63,'' *Sep. Sci. Technol., 18*, 831–841 (1983).
19. P. R. Danesi and R. Chiarizia, ''Kinetics and Mechanism of the Heterogeneous Complex Formation Reaction between Cu(II) and Fe(III) Aqueous Species and a β-Hydroxyoxime in Toluene,'' *J. Phys. Chem., 84*, 3455–3461 (1980).

Received by editor February 25, 1997
Revision received August 1997

Request Permission or Order Reprints Instantly!